



Student Projects Reports
Kinetics of Gases
Graduate Course
Fluid Dynamics
5C1505

Mekanik, KTH
May 2007

Direct Simulation Monte Carlo (DSMC): Introduction and practical use Project in Gas Dynamics course

Antonios Monokrousos & Espen Åkervik

May 7, 2007

1 Introduction to the gas simulation methods

The Navier-Stokes equations commonly encountered in fluid mechanics applications builds on the continuum approximation. When the ratio of the mean free path λ to the macroscopic length scale L , formalised by the non-dimensional Knudsen number $Kn = \lambda/L$, becomes large this approximation breaks down. The macroscopic length scale should be based on the local field (i.e. velocity, pressure, density) to gradient ratio, thereby removing the question on how to defining this length scale for complex flows. For small Knudsen numbers $Kn < 0.1$ the continuum approximation is valid. However for larger Knudsen numbers one has to resort to some sort of methodology which considers interaction between particles. The Boltzmann equation is the accepted mathematical model of a gas flow at the molecular level. Numerically this equation can be solved using conventional CFD techniques, with the velocity distribution function being the obtained solution on a computational grid. Since this is a six-dimensional partial differential equation it quickly becomes computationally heavy. Further the collision terms represented by the right hand side integral is a challenging task to evaluate. An alternative to solving the Boltzmann equation is to employ direct simulation methods, where a large number of simulated molecules are traced in space and time, and their velocities and internal states are modified through collisions and boundary interactions. The most fundamental approach within this class is that of the deterministic *Molecular Dynamics* (MD) in which actual collisions between particles are calculated based on Newton's law or quantum mechanics. Note however that this quickly becomes computationally intractable since as soon as a geometry and the gas characteristics are set there are no tunable parameters, making MD methods applicable only to dense gases. In the next section we will describe briefly the probabilistic approach to direct simulation.

2 The Direct Simulation Monte Carlo (DSMC)

The Direct Simulation Monte Carlo (DSMC) (Bird, 1995) method is suitable for simulating dilute gases by means of a probabilistic approach. The term dilute gas means that a typical molecular spacing δ is much larger than a typical molecule diameter d ,

formally stated as $\delta/d \gg 1$. In terms of Knutsen number this would approximately mean that $\mathcal{O}(0.1) \leq Kn \leq \mathcal{O}(10)$. The fundamental idea of DSMC is to track a large number of statistically representative particles where each of the particles contains a cluster of molecules. The particles motion and interactions are used to modify their positions and velocities.

The DSMC procedure consist of four main stages; move the particles, keep track of the position, perform collisions using probabilistic methods and to sample the flow field. Below these different stages will be described.

Setting physical constants: This is done in subroutines starting with `DATA`, for instance in our zero dimensional test program it is `DATA0S`. Here you can set number density, temperature, molecular mass, diameter and all the time stepping parameters. More information on this is given in section 3.1.

Initialisation: This is performed before the time loop in routines starting with `INIT`. The routine calls `DATA`, seeds the particles in different cells and sub cells also assigning them random velocities by calling `RVELC`. Note that the velocity is always three-dimensional.

Moving particles: At every time step the particles are moved to their new position according to $\vec{r}(t + \Delta t) = \vec{r}(t) + \vec{v}(t)\Delta t$, assuming that no interactions have occurred during this time interval. At this stage boundary conditions are enforced. All of this is performed in the routines starting with `MOVE`.

Indexing: After having moved all the particles according to their velocities a re-indexing is performed in the routines starting with `INDEX`. This implies that in all sub-cells the number of particles are counted, and each molecule are given a specific address.

Collisions: In the DSMC procedure only particles within a cell are paired up in order to perform collisions. Since we are dealing with dilute gases, there is an overwhelming probability that the collisions will be binary, i.e. involving only two particles. Consider a time interval of Δt in a DSMC cell of volume V_c containing N simulated particles each representing F_N number of molecules. The number of collisions that might occur is easily recognised to be $N(N - 1)/2$. This yields that the probability for each of the collisions becomes $P = F_N \sigma_T c_r \Delta t / V_c$ where σ_T is the total collision cross section and c_r is the relative velocity of the pair of particles considered. A straight forward method is now to find collision pairs by considering all $N(N - 1)/2$ potential collisions using a random pick together with the probability P . However due to the large number of particles N and the low probability P this procedure is computationally challenging, requiring a computational time proportional to N^2 . In order to make the computational time linear with N , the DSMC uses the so called NTC (No Time Counter) method in which a normalised probability is introduced

$$P_{\max} = \frac{F_N (\sigma_T c_r)_{\max} \Delta t}{V_c},$$

where $(\sigma_T c_r)_{\max}$ is a precomputed maximum collision cross section of the cell. Based on this a number of representative collisions is computed

$$1/2 N \bar{N} F_N (\sigma_T c_r)_{\max} \Delta t / V_c.$$

Here \bar{N} is a time ensembled average of particles contained in the cell. For each of these possible collisions the procedure now picks a random particle and finds its corresponding sub-cell. Within this sub-cell it picks another random particle so that these

two form a collision pair. The collision is now computed with the probability

$$\frac{\sigma_T C_r}{(\sigma_T C_r)_{\max}}.$$

This essentially means that a random number is compared to the above fraction, and if it is bigger we have a collision, otherwise not. The collisions themselves are modelled as different variants of a hard sphere collision. In the hard sphere approximation, elastic collisions are assumed, yielding a conserved magnitude of the relative velocities of the two particles. It hence becomes necessary only to compute the direction of the particles after the collision, also known as the angle of deflection χ . The angles are computed with random picks for the hard sphere case, but alternative implementations are those of variable hard sphere (VHS) and variable soft-sphere (VSS). The latter two gives better approximations regarding the transfer of momentum and kinetic energy. For a full discussion on the choice of collision model we refer to chapter two in Bird (1995). The collision procedure is implemented in routines starting with COLL.

Sampling: After a number of time step the cell information is sampled in the routines SAMPLE. This is basically a time ensembled average in each cell of quantities such as the number density, the velocities and the temperature.

3 Obtaining the program, operation and all of that

The DSMC package can be download from

<http://www.gab.com.au/CORRIG.HTM>

where also a corrigendum for the different files are included. At the bottom of the page there is a file called DSMCP.EXE. This is a self-extracting zip file containing the source codes. Note that this is a windows application. The individual files can be compiled with any standard Fortran compiler, for instance on the linux machines at the department pgf90 is a common choice. The compiling can be performed by typing

```
bash> pgf90 DSMC0S.FOR
```

producing an executable a.out. You should first add the module pgi by typing

```
bash> module add pgi
```

Important: Check the corrigendum for the program you are running.

Note: For those who do not have windows accessible a zip file can be download from <http://www2.mech.kth.se/~espena/gasdyn/>

3.1 Setting the computational variables

Setting the cell and sub-cell width: Although particles are allowed to cross the borders of the cells, individual collisions occurs with neighbours in the same cell. More specifically, the DSMC uses the sub-cell approach, where local collision rates are based on the individual cells, but the possible collision pairs are restricted to sub cells. A rule

of thumb is that the cell width should be $\Delta x \approx \lambda/3$, where again λ is the mean free path. This quantity can be estimated from that of the hard sphere

$$\lambda = \frac{\bar{c}'/\bar{c}_r}{n\pi d^2} \quad \bar{c}' \approx \bar{c}_r \quad \lambda \approx \frac{1}{n\pi d^2}, \quad (1)$$

where n is the number density, d the molecular diameter and $\bar{c}' = \sqrt{2T_0 k/m}$ is the mean thermodynamic velocity magnitude, with T_0 being the reference temperature (i.e. $T_0 = 273$), k the Boltzmann constant and m the molecular mass. Also note that \bar{c}_r is the average relative velocity magnitude. The sub-cell width should be taken to be small in comparison to λ . Typically this would mean $\Delta x_s \approx 0.1\Delta x$.

Setting the time step: In the DSMC there is no stability limit connected to the choice of the time step Δt . There is however from a physical point of view a limitation given by the mean collision time, essentially saying that the time step should be sufficiently small in order to uncouple the molecular motions and collisions. An estimate to this can be given for a hard sphere as $\Delta t = \lambda\pi/(2\bar{c}')$.

Setting the number of simulated 'particles': Instead of simulating the action of every molecule, the DSMC clusters a large set of molecules, subsequently tracing the each of these clusters as individual 'particles' in time and space. The number of molecules contained in each particle is free for choice but should be chosen in such a manner that statistical fluctuations do not become too large. A reasonable amount of molecules contained in each particle is $10^{14} < F_N < 10^{18}$, yielding it necessary to compute the evolution of between 10^2 and 10^6 particles for a number density of $n = 10^{20}$.

4 Testing the code in 'zero-dimensional' gas

We tested the DSMC procedure in a homogeneous, or 'zero-dimensional' gas. In the language of Bird (1995) a 'zero-dimensional' gas is a gas with no macroscopic gradients. Likewise a 'one-dimensional' gas is a gas with macroscopic gradients in only one direction. Our homogeneous gas simulation code is named DSMC0S. Although the gas is homogeneous a one-dimensional computational domain $x \in [0, 1]$ is considered. The boundary conditions are specular reflections at both boundaries. Two test cases have been simulated in order to illuminate different aspects of the behaviour of the procedure. The first case has an initial equilibrium where the velocity distribution is given by the Maxwell-Boltzmann distribution. The second case has an initial non-equilibrium state where we have set that all particles should have the velocity $(u, v, w) = (407, 0, 0)$. The material properties of the gas are the following; the molecular mass is $m = 5 \times 10^{-26}$, the molecular diameter is $d = 3.5 \times 10^{-10}$ and the number density is $n = 10^{20}$. The number cells is $M_c = 50$ and each cell has 8 sub-cells. The timestep is taken to be 2.5×10^{-5} .

The computational cost of the procedure is mainly determined by the ratio of the number density n to the number of molecules F_N simulated by each particle since the number of simulated particles are $N = n/F_N$. If F_N is too large the simulation is subject to statistical fluctuations and conversely if F_N is too small the computational effort will be very high. The left panel in figure 1 shows the density as a function of x (cell values) after 500 samples starting with initial equilibrium. Statistically in each cell the number density should be 10^{20} . From the dashed line in this plot it can be seen when choosing $F_N = 10^{19}$, implying that only 10 particles are simulated, the statistical fluctuation is large. With decreasing F_N the fluctuations decrease, and a reasonable

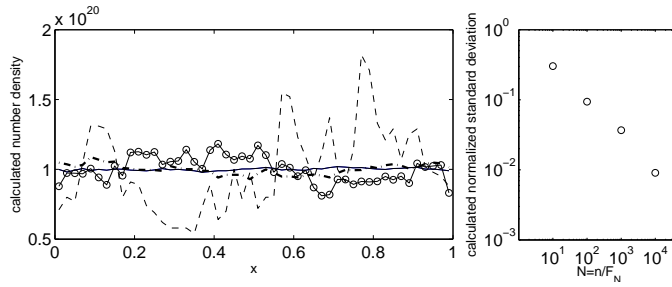


Figure 1: Left panel shows the sampled number density for different number of simulated molecules per particle F_N . Dashed line shows $F_N = 10^{19}$, solid-circles shows $F_N = 10^{18}$, thick dash-dotted line shows $F_N = 10^{17}$ and the thin solid shows $F_N = 10^{16}$. The right panel shows the corresponding standard deviation as a function of $N = n/F_N$.

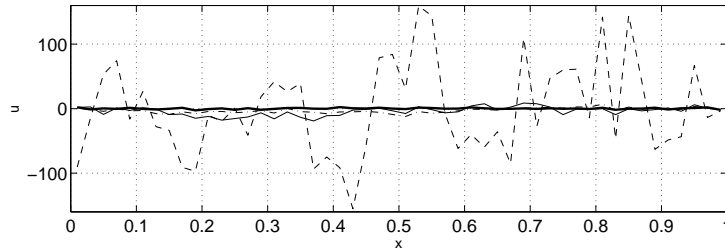


Figure 2: u velocity as a function of x for different sampling intervals starting with initial equilibrium. The dashed line shows u after one sampling, the solid thin line shows after 50 samplings, dash-dotted after 150 samplings and thick solid after 500 samplings. There is four time steps between each sample.

value is $F_N = 10^{17}$, as depicted by the thick dash-dotted line. The right panel shows the standard deviation as a function of N .

Even though starting with initial equilibrium for the case of $F_N = 10^{17}$, the gas is at each instance of time not in equilibrium, and in fact an ensemble average in time at each cell is necessary in order to talk about equilibrium. Figure 2 shows the velocity u in x -direction for different sampling times. Note that there is four time steps between each sampling. After one sample the velocity is varying from cell to cell, as shown by the dashed line. However after more samples the average velocity in each cell tends towards zero.

As a second test case we initiated the gas with a non-equilibrium state $(u, v, w) = (407, 0, 0)$. Figure 3 shows the distribution of velocities among the simulated particles for different samplings. After one sampling almost all particles have the same velocity, but with increasing time the velocity distribution aligns itself with the Maxwell-Boltzmann distribution.

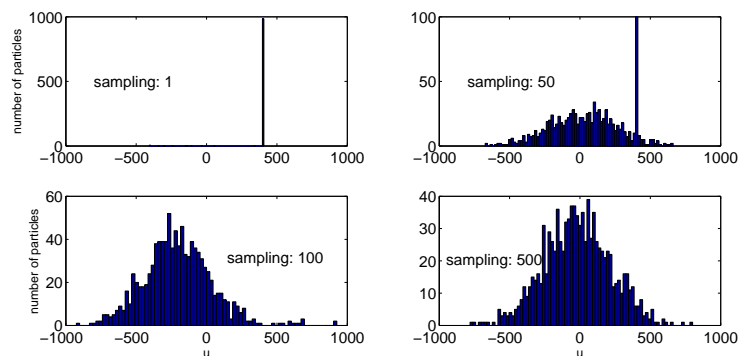


Figure 3: Velocity distribution starting with non-equilibrium for different samples. After one sample almost all particles have the same velocity, but as time goes by the gas aligns itself towards the Maxwell-Boltzmann distribution.

5 List of programs in package

Here follows the list of available codes with a sort description of what each version does:

- DSMC0 Tests the NTC collision sampling procedures in a homogeneous gas mixture of monatomic molecules.
- DSMC0S A version of program DSMC0 for a simple gas.
- DSMC0R Tests the Larsen Borgnakke procedures for the rotational degrees of freedom of diatomic and polyatomic molecules.
- DSMC0V Implements the quantum version of the Larsen-Borgnakke procedures for vibrational excitation.
- DSMC0D Dissociation and recombination of a single species.
- DSMC0F A version of DSMC0 with additional sampling to investigate the properties of the statistical fluctuations.
- DSMC1 A general program for flows with a single spatial variable. The geometry may be plane, cylindrical or spherical.
- DSMC1S A version of DSMC1 for the study of normal shock waves.
- DSMC1T This program models a stagnation streamline flow as a constant area flow with molecule removal at the sides.
- DSMC2 A general program for two-dimensional flows that is restricted to a rectangular flow field and flat surfaces.
- DSMC2A A version of DSMC2 for axially symmetric flows.
- DSMC3 An extension of DSMC2 to three dimensional flows.

References

- BIRD, G. A. 1995 *Molecular Gas Dynamics and the Direct Simulation of Gas Flows*. Oxford Science Publications.

Plane Compressible Couette Flow

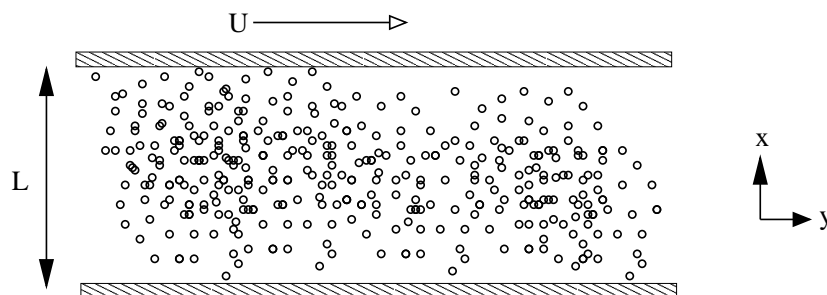
Shervin Bagheri & Johan Ohlsson

May 31, 2007

A Direct Simulation Monte Carlo method (DSMC) was used to simulate the velocity profiles and distribution functions for a gas with various Knudsen numbers. Also the effect of compressibility was examined. The simulation code used was DSMC1. For more information about the code we refer to Bird and Antonios et al.

1 Flow Case and Set-Up

The Couette flow case can schematically be depicted as



The computational domain for the studied flow case is

$$-\infty < y < \infty \quad (1)$$

$$0 < x < 1 \quad (2)$$

$$\dot{y}(0) = 0 \quad (3)$$

$$\dot{y}(1) = v_0 \quad (4)$$

Since the interesting parameters in this case were the Knudsen number and the Mach number, the only physical properties changed in subroutine DATA1 were number density n and number of simulated molecules F_N . The boundary condition v_0 was changed to increase the Mach number. The default values of mass, temperature and molecular diameter were not changed yielding the monatomic gas Argon.

2 Explanation of Results

In Fig. 1 (a) the velocity profile can be seen for various Knudsen numbers and a low Mach number. It can be noticed that for small Knudsen numbers,

which according to the definition of the Knudsen number means a small mean free path compared to the macroscopic length scale, the profile is close to the Navier-Stokes solution of the Couette flow. As the Knudsen number increases the mean free path becomes larger, which means that a molecule will travel longer before a collision occurs. The continuum description of the flow thus breaks down and one has to consider individual particles, which is also done in the DSMC method (even though one 'particle' means many 'real' particles). It can be seen that the profile approaches the half of the wall velocity v_0 . This can physically be explained by considering a molecule moving from the lower wall towards the upper wall. The x-component of the velocity is considered to be zero. When the molecule reflects the upper wall diffusively it will gain an x-component of velocity which is equal to the wall velocity. As the molecule bounces towards the lower wall it will leave all of its x-momentum and once again move upwards in the y-direction without any x-component. In this manner, statistically half the amount of the molecules will have a zero x-component of the velocity and half of them will have the wall velocity as x-component of the velocity thus yielding a macroscopic travelling of $v_0/2$ in the x-direction. This can be seen in Fig. 1 as a 'slip' at the walls. This slip occurs in the *Knudsen layers*, which are of the order of one mean free path in thickness and in which the molecular effects dominates. The Knudsen layers approach zero for the continuum flow since the mean free path becomes negligible compared to the macroscopic length scale.

In Fig. 1 (b) the same plot is made for a higher Mach number. Three things can be seen: The first is that the curves are much more smooth than in the case of a low Mach number. This is due to the fact that the thermal (fluctuating) velocity is much smaller compared to the bulk velocity. Secondly, for a rarefied gas, there is slip at the walls, which could also be seen in the previous case. The third significant property is that the curves are nonlinear, especially near the walls, which is due to the fact that in order for the energy principle to hold, the viscous dissipation generates an energy input which raises the temperature of the gas. But since the temperature is constant at the walls, this means that the temperature will raise in the middle of the channel. And since the viscosity has a temperature dependence, the viscosity will be less in the vicinity of the walls. Now, it can be shown that the shear stress is constant across the flow. In order for this to hold the velocity gradient has to be larger in the vicinity of the walls, which can be seen in Fig. 1 (b).

The figures 2-3 are all simulated at high Mach numbers (which means considerable viscous dissipation in the gas). The (a)-part of Fig. 2 and Fig. 3 both show the distribution of the thermal (fluctuating part) of the velocity for the case of a low Knudsen number. The distribution shows a Maxwellian distribution centered around $c'_x = 0$ and $c'_y = 0$. In the (b)-part of Fig. 2 and Fig. 3 it is interesting to note that when increasing the Knudsen number (thus reducing the number of collisions) we see no more than two Maxwellian distributions, each one reflecting the characteristics of the boundaries - that is, a particle travelling away from the upper plate most probably has a positive streamwise velocity and vice versa.

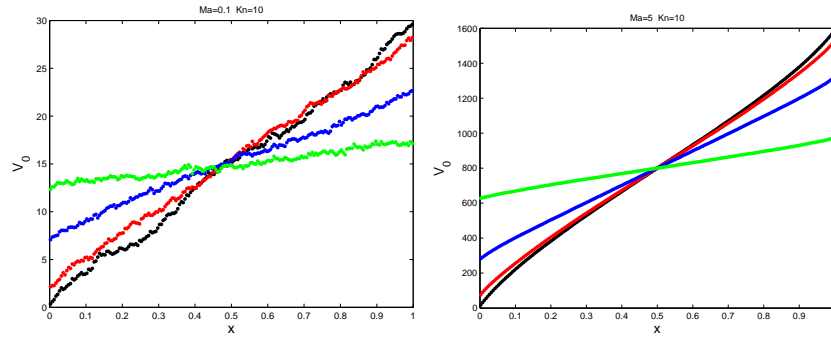


Figure 1: (a) Velocity profiles for different Knudsen numbers and a low Mach number. (b) Velocity profiles for different Knudsen numbers and a high Mach number

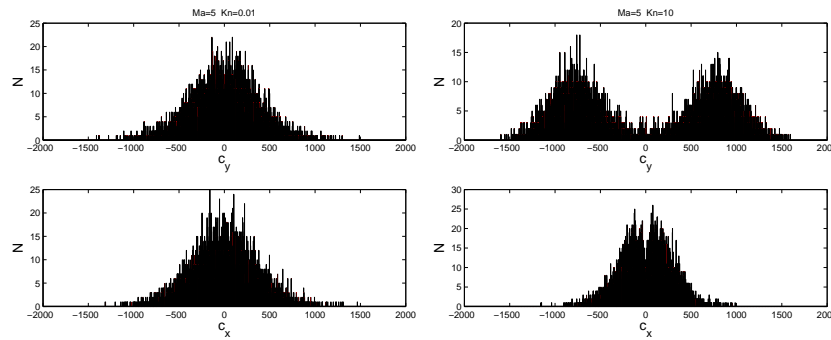


Figure 2: Distribution functions at a high Mach number for (a) low Knudsen number and (b) high Knudsen number.

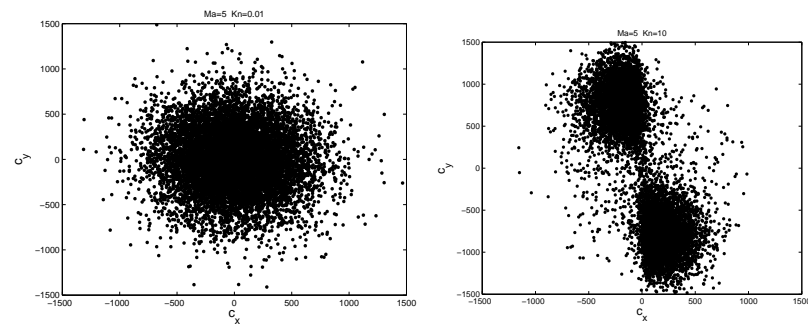


Figure 3: Distribution functions in velocity space for (a) low Kn and (b) high Kn

DSMC simulation of heat exchange between two plates

Tobias Strömgren and Yuan Lin

2007-05-17

1 Theories and methods

The problem is to study the heat exchange between two parallel plates by using the DSMC (Direct Simulation of Monte Carlo) method. Continuum approach is also discussed and compared with the result of DSMC. The free code, DSMC1.FOR of Bird [1] is used for the calculations. The molecules has the same properties as air, but with lower particle density than normal air. It corresponds to air at an elevation of 100 km, i.e. really low pressure.

The heat exchange using the Navier-Stokes approximation is [2] $\Delta\phi_{NS} = -\frac{5}{8} \frac{k}{\omega} \sqrt{\frac{\pi k}{m}} \frac{\sqrt{T_1 + \sqrt{T_1}}}{2} \frac{T_1 - T_2}{L}$. In this problem the temperature profile between the plates will be linear.

The free molecular model is used to calculate the motion of molecules numerically. The simulations was performed using the free software DSMC1.FOR written by G. A. Bird[1]. The formula of heat exchange with the free molecular model is, $\Delta\phi_{free,mol} = \alpha nk \frac{k}{2\pi m} \frac{\gamma+1}{\gamma-1} \frac{\sqrt{T_2 T_1}}{\sqrt{T_1 + \sqrt{T_2}}} (T_2 - T_1)$.

The ratio of hydrodynamic and free molecular heat transfer rate is the following,

$\frac{\Delta\phi_{NS}}{\Delta\phi_{free,mol}} = \frac{5}{8} \frac{\pi}{\alpha} \frac{\gamma+1}{\gamma-1} \frac{(\sqrt{T_1 + \sqrt{T_2}})^2}{\sqrt{T_1 T_2}} \frac{\lambda}{L}$ which shows that in high Kn number region ($\lambda > L$), improper use of hydrodynamic formulas in free molecular situation might lead to gross overestimations of the heat transfer rate.

2 Results

By changing the distance between the two plates, we get temperature profiles for different Kn numbers as figure 1. The temperature boundary conditions are, $T_1 = 273K$, and $T_2 = 373K$. Fig 1(a) shows that when $Kn = 0.01$, the free molecular method give almost the same solution as the 'Navier-Stokes' approach. When Kn increases, the rate (dT/dx) of heat exchange decreases. Fig 1(b) shows that when Kn decreases, the density of particles increases at the plate with lowest temperature, which agrees with the relation that under equilibrium conditions the pressure is constant, that is $n_1 T_1 = n_2 T_2$.

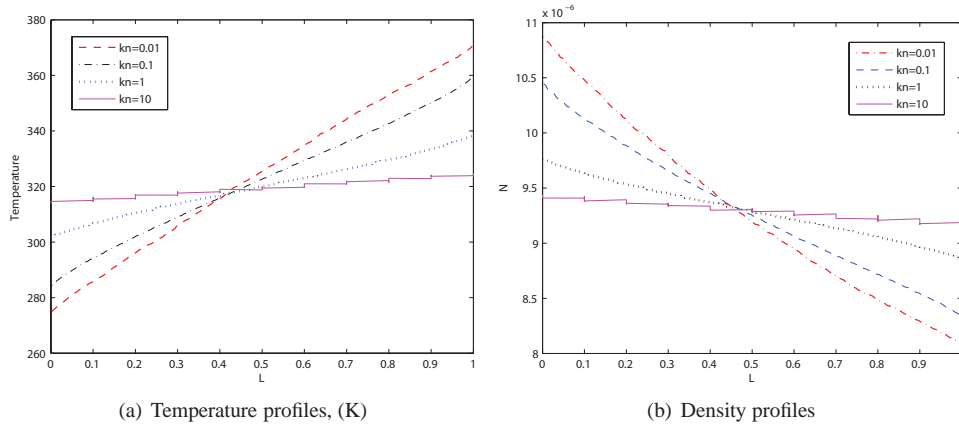


Figure 1: Temperature and density when temperature difference is 100K

Figure 2 shows the velocity distribution of molecules when temperature difference is 1000K. Fig 2(a), $Kn=0.01$, shows that the velocity distribution is isotropic in both x-, and y-directions. Where the x-direction is normal and the y-direction is parallel to the plates. Fig 2(b) shows that when $Kn=10$, the y-component of the velocity distribution is symmetric, but the x-component of the velocity distribution is not symmetric. In figure 3 where the velocity in the x-direction is shown in a histogram, it is even more clear that for large Knudsen numbers more particles are moving in the direction from the warm plate to the colder plate. For $Kn=0.01$ there is a Maxwellian distribution centred around $c_x = 0$ but this is no the case for $Kn=10$.

Our calculations have shown that the 'Navier-Stokes'- and the free molecular approach overlap for $Kn < 0.01$, as Kn increases the difference between the free molecular model and the 'Navier-stokes' approach increases. As stated earlier Navier-Stokes works fine for $Kn < 0.01$. One can also say that rate of heat-transfer decreases with increasing Kn .

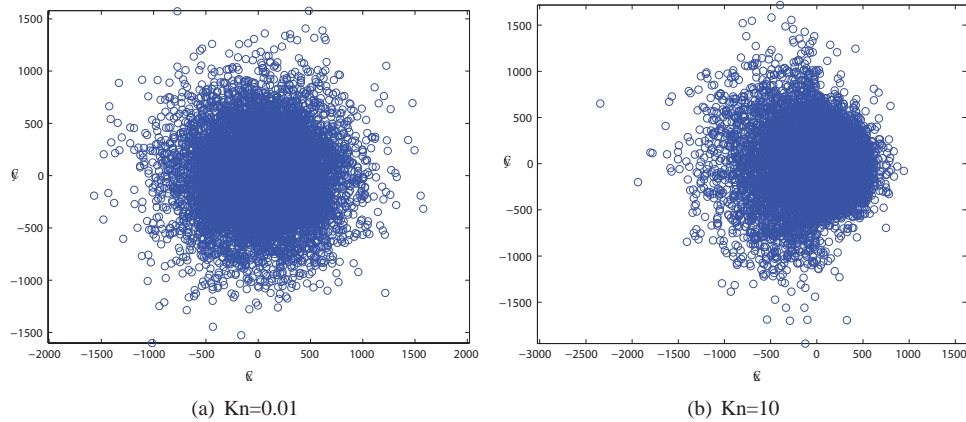


Figure 2: Velocity distribution when temperature difference is 1000K, (m/s)

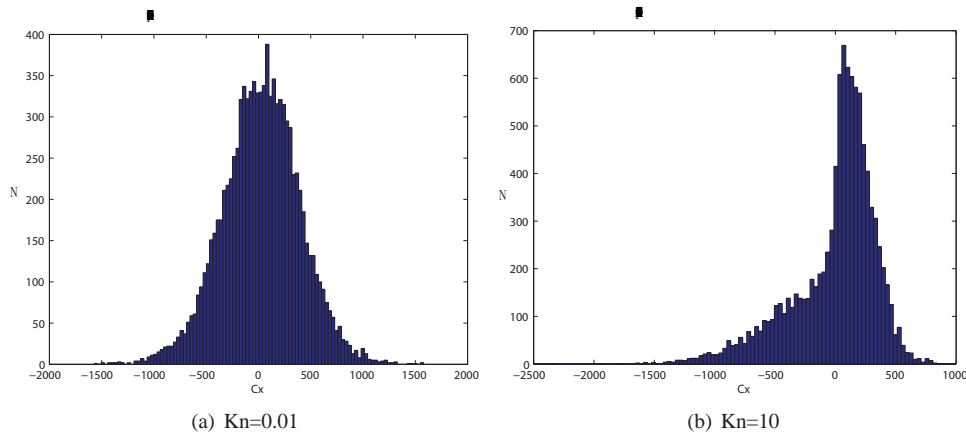


Figure 3: X-component velocity distribution when temperature difference is 1000K, (m/s)

References

- [1] G. A. Bird "Molecular Gas Dynamics and the Direct Simulation of Gas Flows" *Oxford Science Publications, UK*, 1994
- [2] T. I. Gombosi "Gaskinetic theory", *Cambridge Atmospheric and Space Science Series, UK*, 1994, p. 250-253

The Hypersonic Flat-Plate Boundary-Layer Flow - Project Report, Course 5C5105, part III

Lars-Uve Schrader and David Tempelmann

Linné Flow Centre, KTH Mechanics, 100 44 Stockholm, Sweden schrader@mech.kth.se,
david@mech.kth.se

1 Introduction

This report deals with results obtained from Monte-Carlo Direct Simulations (DSMC) of the hypersonic flow over a flat plate. In the first section general features of hypersonic boundary-layer flows, the limits of the continuous-fluid assumption and some aspects of molecular kinetics will be discussed. The second part will be about the set-up of the simulations and the study cases. In the third part the most interesting results will be compiled.

2 Hypersonic boundary-layer flow

Within hypersonic boundary layers the large amount of kinetic energy is transformed into internal energy due to viscous effects (viscous dissipation). Thus, the temperature increases significantly, meaning that the viscosity in turn will increase and the density will decrease. Both effects make the hypersonic boundary layer grow faster than at lower speeds. A relation can be given as $\delta/x \propto M_\infty^2/\sqrt{Re_x}$ [1].

The thick boundary layer causes a particularly large displacement of the streamlines - especially of those close to its edge. Hence, the boundary layer may be seen as an obstacle, forcing the outer streamlines to change direction. In super- or hypersonic flows no information about this obstacle can, however, travel upstream of the leading edge of the plate unless there is a shock wave.

The outer inviscid flow is greatly affected by the thick boundary layer, e.g. through the shock. These changes feed back and influence the growth of the boundary layer as well. This phenomenon is called viscous interaction.

At low Reynolds numbers the shock and the boundary layer can merge. Then the latter can no longer be described by conventional theory.

Especially close to the leading edge the local Knudsen number based on the chordwise coordinate becomes very large; towards the leading edge it tends to infinity ("leading-edge problem"). Low-density effects become therefore important in particular in the leading-edge vicinity. For low-density flows the Knudsen layer at the wall might no longer be negligible. In this layer only molecule-wall collisions occur but no inter-molecular collisions, which results in wall velocity slip. At even larger Knudsen numbers the assumption of a continuous fluid may lose its validity.

3 Numerical set-up and simulation cases

The hypersonic flat-plate boundary-layer flow is treated as a two-dimensional problem. The bulk velocity vectors are confined to the x, y -plane; however, for the thermal velocity a spanwise component is allowed as well.

The computational domain consists of 100 cells of 1 cm width in streamwise direction and 60 cells of 1cm height in wall-normal direction. These cells are sub-divided into 2x2 sub-cells.

The flat plate coincides with the lower boundary $y = 0$ and is located in the streamwise interval $x = [0.1, 1.0]m$, see Figure 1.

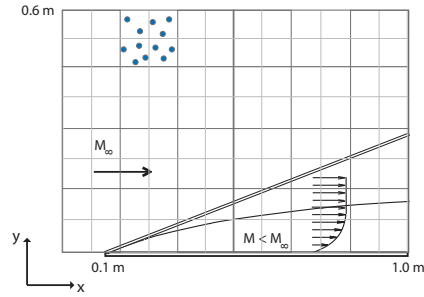


Fig. 1. The hypersonic flat-plate boundary-layer flow: A sketch of the computational domain

40000 particles representing of the order of 10^{15} molecules are distributed among the sub-cells. At the inflow boundary $x = 0$ the particles have a uniform bulk velocity parallel to the plate and initially random thermal velocities. At the outflow plane a stream condition is specified. The boundary condition along the line $y = 0$ is twofold: Upstream of the leading edge a symmetric boundary condition is specified, being equivalent to a specular reflection of the particles at their mirrored images. Along the plate surface a diffusive-reflection condition is set in order to meet the reflection behaviour at a realistic rough wall.

Four different cases are studied in the following: The "standard case" with Mach number $M = 4.0$ and Knudsen number $Kn = 0.02$, two low-number density cases for which the Knudsen number is changed to $Kn = 0.04$ and $Kn = 0.2$, respectively, and a high-Mach number case with $M = 6.0$ and $Kn = 0.02$. The most interesting results are compiled in the next section.

4 Results

M = 4, Kn = 0.02 ($\lambda = 1.8cm$).

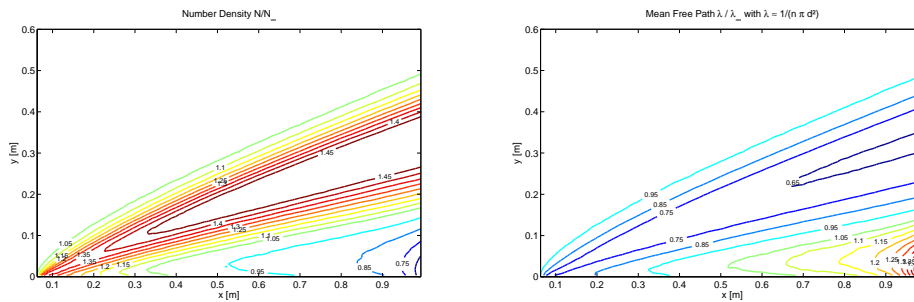


Fig. 2. Distribution of the number density (left) and the dimensionless mean free path (right) in the flow field. Across the shock the number density increases strongly, whereas it decreases within the boundary layer due to its high temperature and due to downstream expansion.

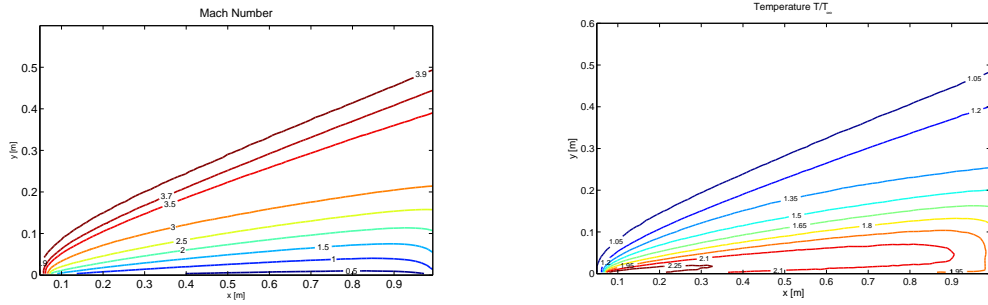


Fig. 3. Left: Distribution of the Mach number; right: The dimensionless temperature (based on the free-stream temperature $T_\infty = 300K$) in the flow field. Clearly, the temperature is highest within the boundary layer, especially close to the wall. Also a temperature slip can be identified here.

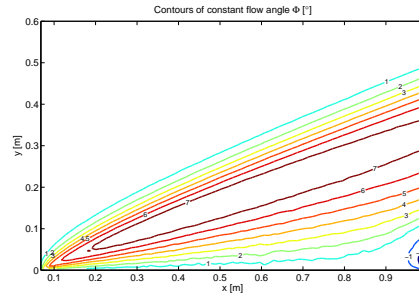


Fig. 4. Lines of constant inclination angle of the streamlines. The boundary-layer edge is located roughly where the flow angle is maximum. The negative streamline angle in the boundary layer at the outflow plane is due to the outflow boundary condition that turned out to be appropriate only for an outflow Mach number of $M_{out} > 2$ [2]. In the boundary layer the Mach number at the outflow boundary is, however, locally lower than 2.

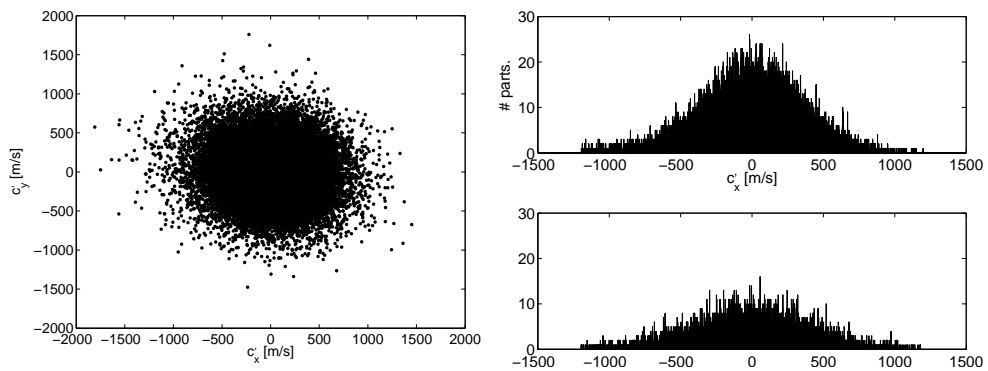


Fig. 5. The distribution of the thermal velocity. Left: Velocity-distribution function in the streamwise-normal velocity plane. Right: The distribution of the streamwise component of the thermal velocity. Top: Within the interval $y = [0.4, 0.6]m$ ("upper stripe"); bottom: Within the interval $y = [0, 0.2]m$ ("lower stripe"). The lower stripe contains the boundary layer and parts of the shock. Thus, the deviation of the velocity distribution from the Maxwell-Boltzmann distribution is larger here than in the upper stripe.

$M = 4$, $Kn = 0.2$ ($\lambda = 18\text{cm}$).

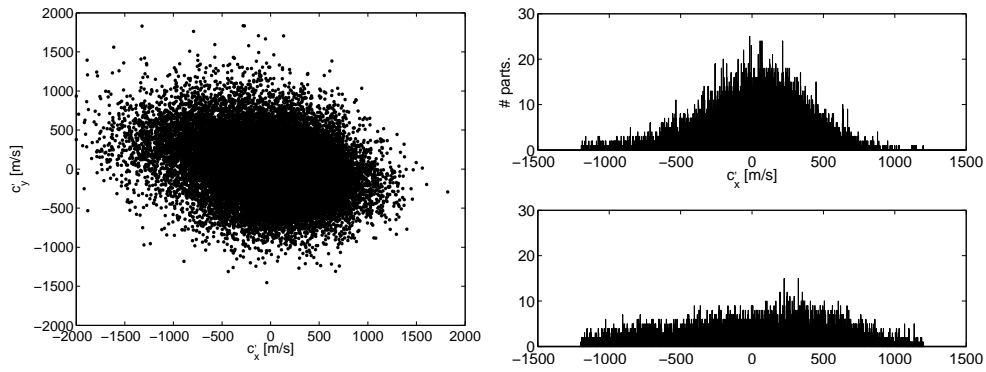


Fig. 6. The distribution of the thermal velocity for the low-density case, $M = 4$, $Kn = 0.2$. Left: Velocity-distribution function in the streamwise-normal velocity plane. Right: The distribution of the streamwise component of the thermal velocity. Top: Within the interval $y = [0.4, 0.6]m$ ("upper stripe"); bottom: Within the interval $y = [0, 0.2]m$ ("lower stripe"). In comparison to the standard case the all-over distribution (left) and the distribution of the streamwise thermal-velocity component is less symmetric and deviates more from the Maxwell-Boltzmann distribution.

Comparison between the four cases.

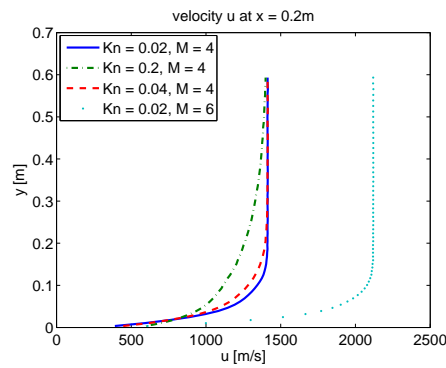


Fig. 7. Comparison of the wall-normal profiles of the streamwise velocity for the standard case ($M = 4$, $Kn = 0.02$), the two low-density cases ($M = 4$, $Kn = 0.04/0.2$) and the high-Mach number case ($M = 6$, $Kn = 0.02$). The relative velocity slip based on the free-stream velocity is largest in the lowest-density case, when the Knudsen layer on the wall is particularly thick. The boundary-layer thickness is smaller in the $M = 6$ case, which is in contrast to the relation $\delta/x \propto M_\infty^2/\sqrt{Re_x}$. However, this equation does not include viscous interaction between the boundary layer and the outer flow, whereas this effect is included in the DSMC method.

References

1. J. D. Anderson. Hypersonic and High Temperature Gas Dynamics. *McGraw-Hill*, 1989.
2. G. A. Bird Molecular Gas Dynamics and the Direct Simulation of Gas Flows. *Oxford Science Publications*, 1995.

Flow towards an inclined flat plate

- student project report

Ola Lögberg & Bengt Fallenius

1 Introduction

In this report the supersonic flow around an inclined flat plate is calculated using the direct simulation Monte Carlo (DSMC) method. This method can be used when the Navier-Stokes equations no longer is applicable, *i.e.* when the Knudsen is in the region of 0.1 and higher. In this project the two-dimensional DSMC2 code, developed by G.A. Bird, was used.

2 Parameters

The DSMC2 code had a number of parameters to specify the domain, the number of cells and subcells, the medium and the plate.

2.1 Domain

The computational domain length (x) and height (y) was set to 1 m and 0.6 m, respectively, and divided into 100 cells in the x -direction and 60 cells in the y -direction. Each cell was further divided into 2x2 subcells. The domain was specified to have free in- and outflow through all boundaries.

2.2 Flow

The medium was set to Argon and the Mach number was $M = 4$ for all angles. The temperature of the flow was set to 300 K, the Knudsen number $Kn = 0.09$ and the number of particles and number density was 40 000 and 1×10^{20} , respectively. This gives a mean free path $\lambda = 1.8$ cm, which corresponds to an altitude of 100 km.

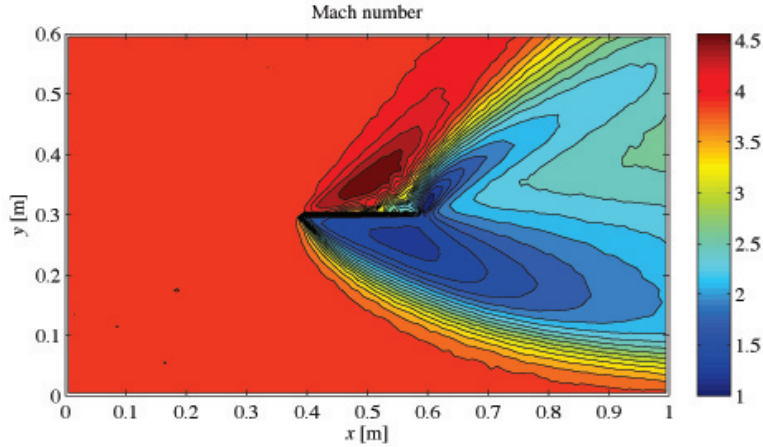


Figure 1: Contours of constant Mach number at 30° angle of attack.

2.3 Plate

The plate was defined by two surfaces and their normals. In the current setup the surfaces were located between cell number 40 and 60 in the x -direction and along the lower boundary of row number 31 and the upper boundary of row number 30 in the y -direction with the normals pointing upwards and downwards, respectively. The angle of the plate was specified by adjusting the x - and y -components of the flow velocity vector. Three different angles were examined: $\alpha = 15, 30$ and 45 degrees. The temperature on the surface was set to ambient on the downstream side while the upstream side was set to have the stagnation temperature of the flow.

3 Results

Only results from an angle of attack of 30 and 45° are shown.

In figure 1 the shock waves under the leading edge and over the trailing edge can clearly be seen. The two accompanying Prandtl-Meyer expansions are also captured reasonably well, when compared to the text book illustration in figure 2.

When the angle of attack is increased to 45° the leading edge shock wave detaches from the surface as seen in figure 3. This agrees well with classical theory that states that the detachment deflection angle at $M = 4$ is 39° . Since the shock wave is attached at 30° , the detachment angle predicted by the simulation is between 30 and 45° . In figure 4 an experimental realisation

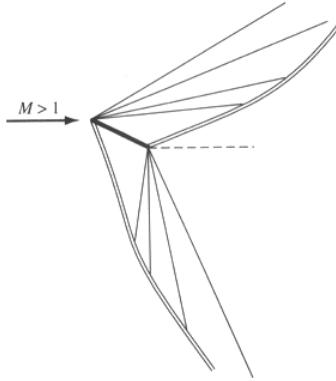


Figure 2: Shock waves and expansions around an inclined surface in a supersonic free stream.

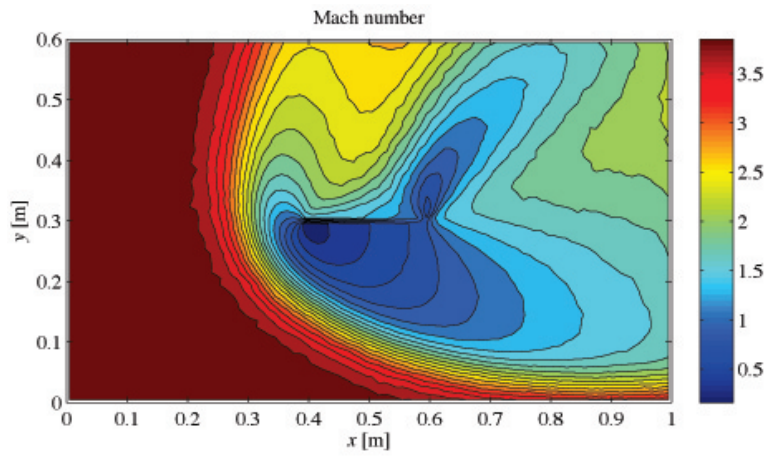


Figure 3: Contours of constant Mach number at 45° angle of attack.

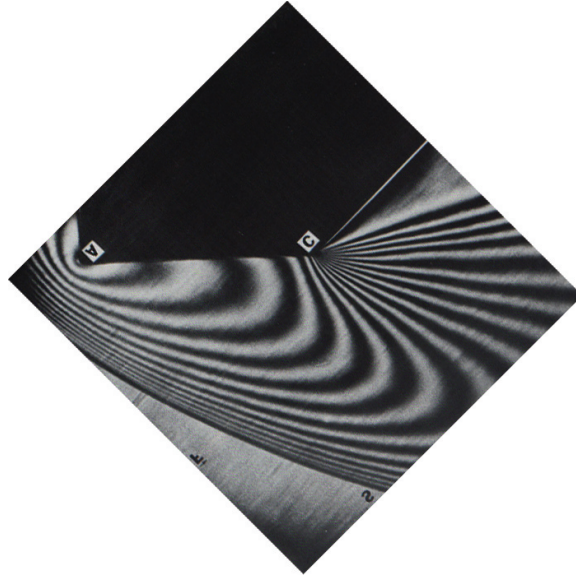


Figure 4: A detached shock wave on a 45° wedge at $M = 2.5$. (Milton van Dyke, "An album of fluid motion")

of a similar case is shown.

In figure 5 the velocity component parallel to the lower surface is plotted. The width of the shock wave depends on how it is defined, but it seems to be approximately 3 mean free paths.

The difference between the components of the translational temperature provide a measure of the departure from local equilibrium at a position in the flow. In figure 6 this is shown along the same row of cells as in figure 5. Upstream of the shock wave the temperature components are of the same magnitude. In the shock T_y , which is the temperature component most normal to the shock wave, increases abruptly. The two other components increases more gradually. In the expansion T_y is still the component that is affected first.

4 Conclusions

DSMC2 manages to capture the main flow phenomena of the three presented cases. Note especially the good agreement with classical theory when the leading edge shock wave is detached at 45 degrees. The translational temperature equilibrium is lost in the shock wave.

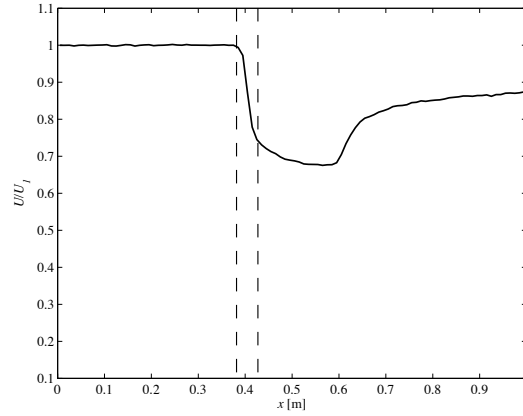


Figure 5: U/U_1 in the first row of cells below the plate at 30° angle of attack. The distance between the dotted lines is 3 times the mean free path λ .

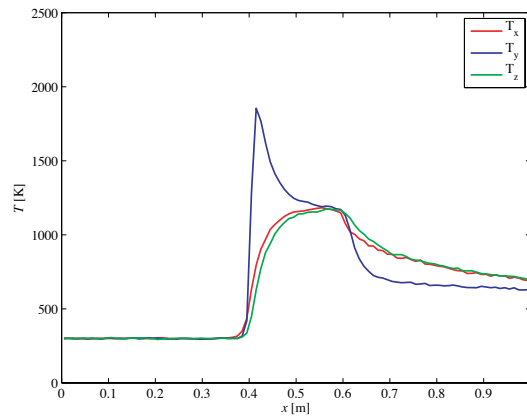


Figure 6: The translational temperature in the x , y and z direction in the first row of cells below the plate at 30° angle of attack.

Direct Simulation Monte Carlo of gas flow in a cylinder

F. Hellström and A. Svärd

May 29, 2007

1 Introduction

When the ratio of the mean free path, λ of the gas to the characteristic length of the flow L , the Knudsen number (1) exceeds values of approximately 0.1 the flow can no longer be described using a continuum approach, and the well known Navier-Stokes equations are not valid.

$$Kn = \frac{\lambda}{L} \quad (1)$$

Instead, the behaviour of the flow is described by the Boltzmann equation, which in this study has been solved by the Direct Simulation Monte Carlo (DSMC) method. The flow case is a Poiseuille flow driven by a gravitational volume force in a cylindrical pipe. The results have been compared with an analytical solution and the agreement was found to be good for low Knudsen numbers and moderate driving force.

2 Analytic solution

For fully developed flow with constant pressure, $U_r = 0$, $U_\theta = 0$, $U_z = U_z(r)$ and gravitation in z -direction the velocity profile for pipe flow can be described by an analytic solution (2)

$$U_z = \frac{R^2 - r^2}{4\mu} \rho g \quad (2)$$

where r is the radial coordinate, R is the pipe radius, μ is the viscosity, ρ the density and g the gravitation. This equation can be modified to account for slip flow at the walls (3),

$$U_z = \frac{(1 + \frac{4}{3} \cdot Kn) \cdot R^2 - r^2}{4\mu} \rho g \quad (3)$$

As can be seen in equation (3), the velocity will increase with increasing Knudsen-number if the driving force $\rho \cdot g$ is constant.

3 Computations

In this study of the gas flow in a pipe the Direct Simulation Monte Carlo approach is used to numerically solve the Boltzmann equation. The used code is the DSMC1 developed by Bird [1] with the assumptions mentioned above. Since the DSMC1 only can handle flow gradients in the r -direction, it had to be modified to be able to handle a gravitational force in the z -direction.

6 different cases have been computed, 3 with different Mach numbers and 3 with different Knudsen numbers. The Mach numbers were varied by varying the gravitation. A gravitation of $2.5 \cdot 10^4 m/s^2$ gave a Mach number of 0.23, while a gravitation of $2.5 \cdot 10^5 m/s^2$ and $2.5 \cdot 10^6 m/s^2$ gave Mach number of 1.45 and 2.3, respectively. For these cases, the number density was kept constant, and hence the Knudsen number.

For the cases with different Knudsen number, the Knudsen number where varied by varying the number density while keeping the driving force, in these cases $\rho \cdot g$ constant. The number density for the three different cases were $n = 9.5 \cdot 10^{22}$, $n = 9.5 \cdot 10^{20}$, and $n = 9.5 \cdot 10^{19}$ which resulted in a Knudsen number of $Kn = 0.001$, $Kn = 0.1$, and $Kn = 1$, respectively.

The gas was treated as a mono-atomic gas. The pipe radius was 0.01 meter and at the pipe wall, a solid wall boundary condition was applied.

4 Results

In figure 1 the Mach number distribution over the pipe radius is shown for a low Knudsen number, $Kn = 0.001$, and varying driving force. As expected, the overall Mach number is lower in the case of a lower driving force. In the case with the lowest driving force the centerline Mach number is only slightly above 0.2. The flow can be considered incompressible and the agreement with the analytic solution is good. The other two cases show centerline Mach numbers well above 1. This implies that the flow is far from incompressible and the agreement with the analytical solution is growing poorer. The simulated density and temperature results are essentially constant in the low Mach number case but show gradients in the radial direction for the higher Mach numbers. The product between density and temperature is however constant for all three cases.

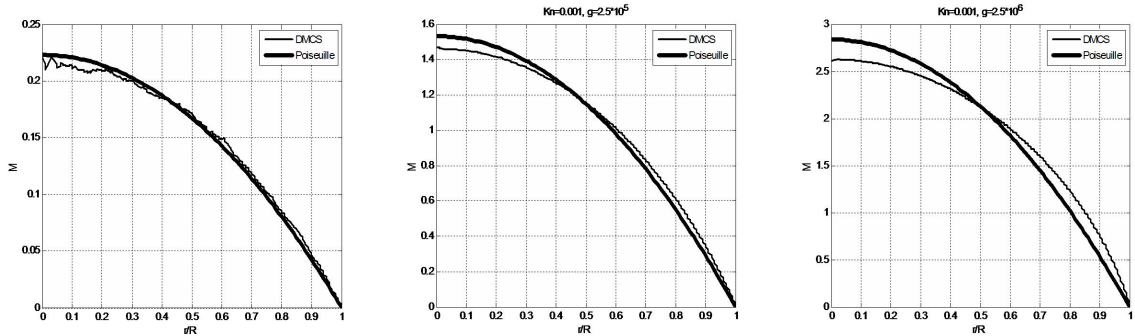


Figure 1: The Mach number distribution over the pipe radius for $Kn=0.001$. The leftmost figure represents a case with low driving force, ρg and the driving force increase to the right.

Figure 2 show the Mach number distribution over pipe radius for three cases with the same driving force at different Knudsen numbers. It is clear that the Mach number increases with increasing Knudsen number. This is partly due to slip but mostly owing to the fact that fewer collisions take place at high Knudsen numbers so the available kinetic energy is concentrated in the axial direction. The low Knudsen number case show good agreement with the analytical solution whereas the higher Knudsen numbers show increasingly poorer agreement as assumptions made in the analytical solution begin to fail. There is also a significant slip at $Kn=0.1$ and $Kn=1$ that can not be detected at $Kn=0.001$.

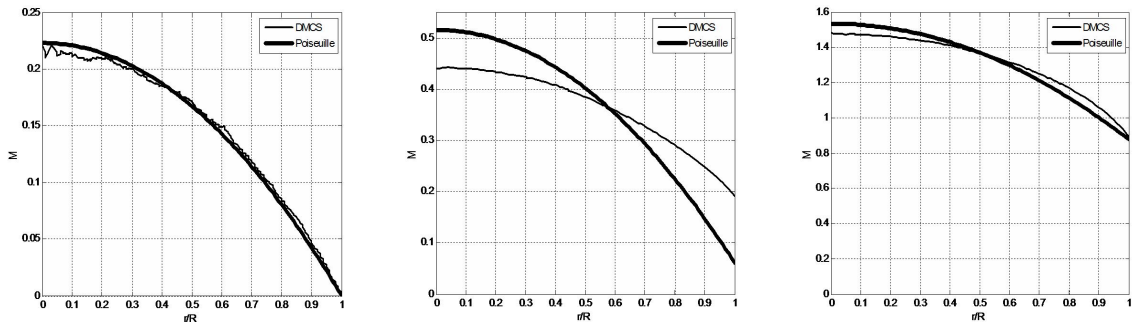


Figure 2: The Mach number distribution over the pipe radius for constant ρg . Left $Kn=0.001$, middle $Kn=0.1$, right $Kn=1$.

References

- [1] Bird G.A., Molecular Gas Dynamics and th Direct Simulation of Gas Flows, Oxford Science Publications, 1994

The shock structure of a monoatomic gas
FMGS 07

Tomas Muld and Olle Bodin

May 31, 2007

1 Problem Setup

The program used for simulation the shock with a Direct Simulation Monte Carlo (DSMC) method was DSMC1S.FOR. The setup for this programs was that Argon was the gas simulated. The initial temperature before the shock is 293 K, which also gives a speed of sound at 318.65 m/s. The number density is 10^{20} and before the shock the density ρ is $6.6 \cdot 10^{-6}$ kg/m³. The computational domain is 0.6 m divided into 300 cells with 6 subcells. This is a large domain for a shock, but since the number density is so small the mean free path is large, $\lambda_1 = 0.019$ m, the shock is wider. That these values are large does not really matter since the results are all normalized to be able to compare the analytical with the DSMC solution. In the program the x-axis is in the direction across shock. The reference frame is moving alongside the shock, so that the shock will always be in the middle.

2 Analytical solution

To objective was to compare DSMC with an analytical solution to the shock profile. The analytical solution is derived from the equations for conservation of mass, momentum and energy. These must be satisfied throughout the shock. The equations can be simplified under the assumption that the shock is weak, weak means that: $M_1^2 - 1 \ll 1$. Where M_1 is the Mach number in front of the shock. With this assumption the conservation equations can be linearized. Solving for the velocity u gives the result:

$$\frac{u - u_2}{u_1 - u_2} = \frac{1}{1 + e^{G \frac{u_1 - u_2}{C_1 \lambda_1}}}$$

Where u_1 and u_2 are the velocities before and after the shock, G is a constant depending on Pr and γ , C_1 is the speed of sound before the shock and λ_1 is the mean free path before the shock. For a monoatomic gas, like Argon that we are using, the constant $G = \frac{8}{7}$. The velocities before and after the shock is taken from the result of the DSMC simulation. Another property that we are interested in is the density across the shock. This could easily be calculated from the conservation of mass, when the velocity has been computed. The conservation of mass looks like:

$$\rho u = \rho_1 u_1$$

The last property that we looked at with the analytical solution is the entropy. For an monoatomic gas at room temperature the dimensionless entropy S can be expressed as:

$$S = \frac{s - s_1}{C_v} = \ln \left(\left(\frac{u}{u_1} \right)^{\frac{2}{3}} \left(1 + \frac{M_1^2}{3} \left(1 - \left(\frac{u}{u_1} \right)^2 \right) \right) \right)$$

This was used for calculating S for the analytical solutions.

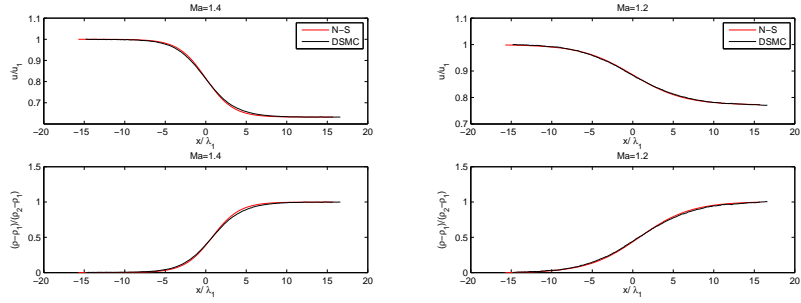


Figure 1: Mach number and density for two low Mach number cases.

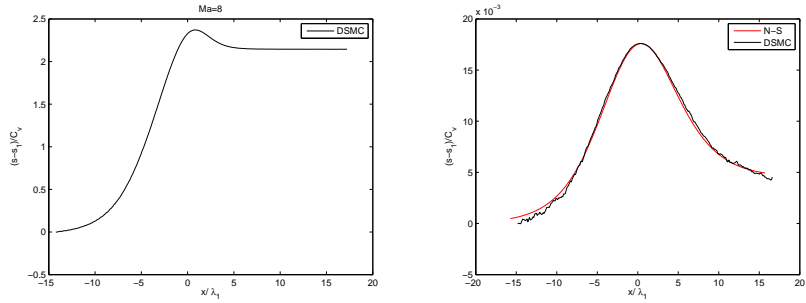


Figure 2: Entropy change for a high and a low Mach number case.

3 Results

A number of different Mach numbers were simulated and compared with analytical Navier-Stokes solutions. The smallest Ma tested was 1.2 and the largest 8. Below a Ma of 1.2 accurate results could not be obtained. To go above Ma=8 was not considered necessary as a clear trend could be observed already in the tested range which was believed to be correct. In figure 1 velocity and density plots for the two low speed cases can be seen, these show how the DSMC and N-S results start to diverge. The shock width was found to be monotonically decreasing for N-S while for DSMC a clear minimum width was observed at a Ma = 3, see figure 4. The same trend could be observed in the temperature and entropy change over the shock. A clear overshoot could be observed in the entropy change for both N-S and DSMC, see figure 2. The entropy can decrease locally in a non-closed system as in the shock, however, globally the entropy increases making it non-isentropic. The translational temperature is related to the kinetic energy of the molecules and if they are out of phase the gas is in a non-equilibrium state. At all tested Mach numbers the component parallel to the flow is out of phase with the other components as they are delayed in the shock but in phase before and after, see figure 3.

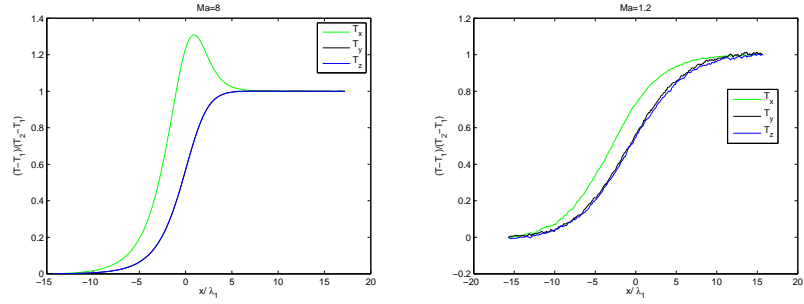


Figure 3: Translational temperature components for a high and a low Mach number case.

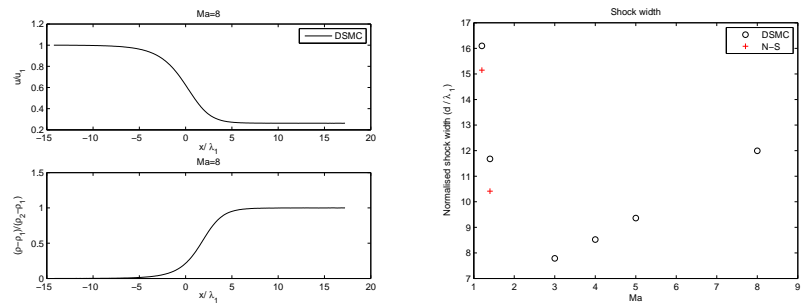


Figure 4: High Mach number shock, left, and shock width as function of Mach number, right.

4 Conclusions

For strong shocks there are discrepancies between N-S and DSMC regarding the flow in the shock. Due to high local Knudsen numbers the N-S equation break down and will not be able to resolve the macroscopic gas properties correctly in the shock. Unfortunately no analytical Navier-Stokes solution valid at high Mach number is available for comparison with the DSMC results. It is however believed that Navier-Stokes will not, as DSMC, have a minimum at about Mach 3, whereafter it will grow again. For DSMC the translational temperature components were found to be in non-equilibrium in the shock as the components not parallel to the flow are delayed compared to the one in the flow direction.

Flow in front of a moving piston

Allan Carlsson & Thomas Kurian

May 31, 2007

The gas flow in front of a moving piston is simulated with a Monte Carlo algorithm. Results are obtained for various velocities of the piston and are compared with theory from ordinary gas dynamics.

Problem formulation

A piston is located at $x = 0$ in a tube, see figure 1. On the right side of the piston, *i.e.* $x > 0$, the tube is filled with the monatomic gas Argon. The initial temperature and number density of the gas is $T_0 = 273$ K and $n = 1 \cdot 10^{20}$, respectively. At time $t = 0$ the piston is given an instantaneous constant velocity c_p in the x -direction. When the piston moves a shock wave is generated in front of the piston. The shock propagates with the velocity $c_{sw} > c_p$.

Theoretical preliminaries

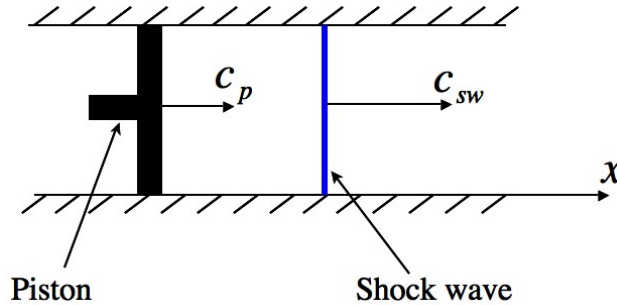


Figure 1: Schematic figure of flow situation.

In order to use normal shock relations the reference frame of the problem is changed to a frame where the normal shock is standing still. The streamwise position of the tube is now x' , where $x' = 0$ at the location of the shock. Properties upstream, *i.e.* $x' > 0$, and downstream of the shock are denoted by index 1 and 2, respectively. In this frame

$$\frac{u_1}{u_2} = \frac{(\gamma + 1)M_1^2}{2 + (\gamma - 1)M_1^2} \quad (1)$$

where $M_1 = c_1/a_0 = c_{sw}/a_0$ and the specific heat ratio $\gamma = 5/3$, see for instance Andersson (2003). The speed of sound a_0 is evaluated at $t = 0$. With $u_1 = c_{sw}$ and $u_2 = c_{sw} - c_p$ there are 3 solutions, when solving for c_{sw} . One solution is $c_{sw} = 0$ and is disregarded. Only one of the remaining two solutions is positive and is given by

$$c_{sw} = \frac{c_p(\gamma + 1)}{4} + \sqrt{\left[\frac{c_p(\gamma + 1)}{4}\right]^2 + a_0^2} \quad (2)$$

| Case | c_p (m/s) | M_p |
|------|-------------|-------|
| 1 | 150 | 0.5 |
| 2 | 308 | 1.0 |
| 3 | 550 | 1.8 |
| 4 | 1000 | 3.3 |
| 5 | 1500 | 5.0 |
| 6 | 2300 | 7.5 |

Table 1: List of cases investigated

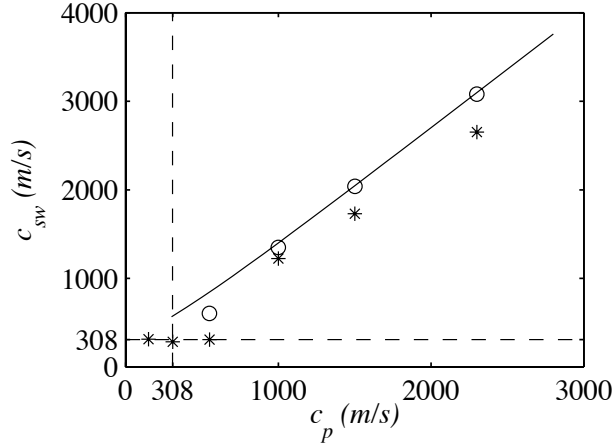


Figure 2: Speed of shock wave and disturbances

According to equation (2) there is a shock also for small c_p . In the limit $c_p \rightarrow 0$ the velocity of the shock $c_{sw} \rightarrow a_0$. In the other limit $c_p \rightarrow \infty$ the velocity $c_{sw} \rightarrow c_p(\gamma + 1)/2 = 4c_p/3$.

Numerical simulations

A total of 6 cases were simulated varying the speed of the piston. The cases are listed in table 1.

As the piston is given a velocity a disturbance is generated, propagating in front of the piston. Between the piston and the disturbance there is a region where the fluid has a higher density and pressure than the undisturbed fluid in front of the disturbance. In figure 2 the speed of the initial disturbance is denoted by stars. The solid line is given by equation 2 and the open circles are the speed of the location where the local mach number $M = 1$. In order to get $M = 1$ the piston has to move with $M_p > 1$. This is due to the fact that as soon as the piston starts to move the temperature at the piston rises and thus so does the speed of sound. This is the reason why the open circles are only reported for the cases with larger c_p . For large c_p the open circles coincide well with the analytical prediction and the slope approaches an asymptotic value of $c_{sw}/c_p = 1.33$, consistent with theory. However, for smaller c_p the data starts to deviate. This deviation could possibly be due to some numerical issues or perhaps the simulation just needs to be run for longer times.

Figure 3 shows the parameters of temperature, density and M along the pipe at two different time steps for 2 different speeds. For the slower speed we see that the disturbance grows ahead of the piston and that this disturbance region increases with time. This disturbance is traveling at the speed of sound which in this case is faster than the piston. For the higher speed we see that the disturbance reaches a level higher than $M = 1$,

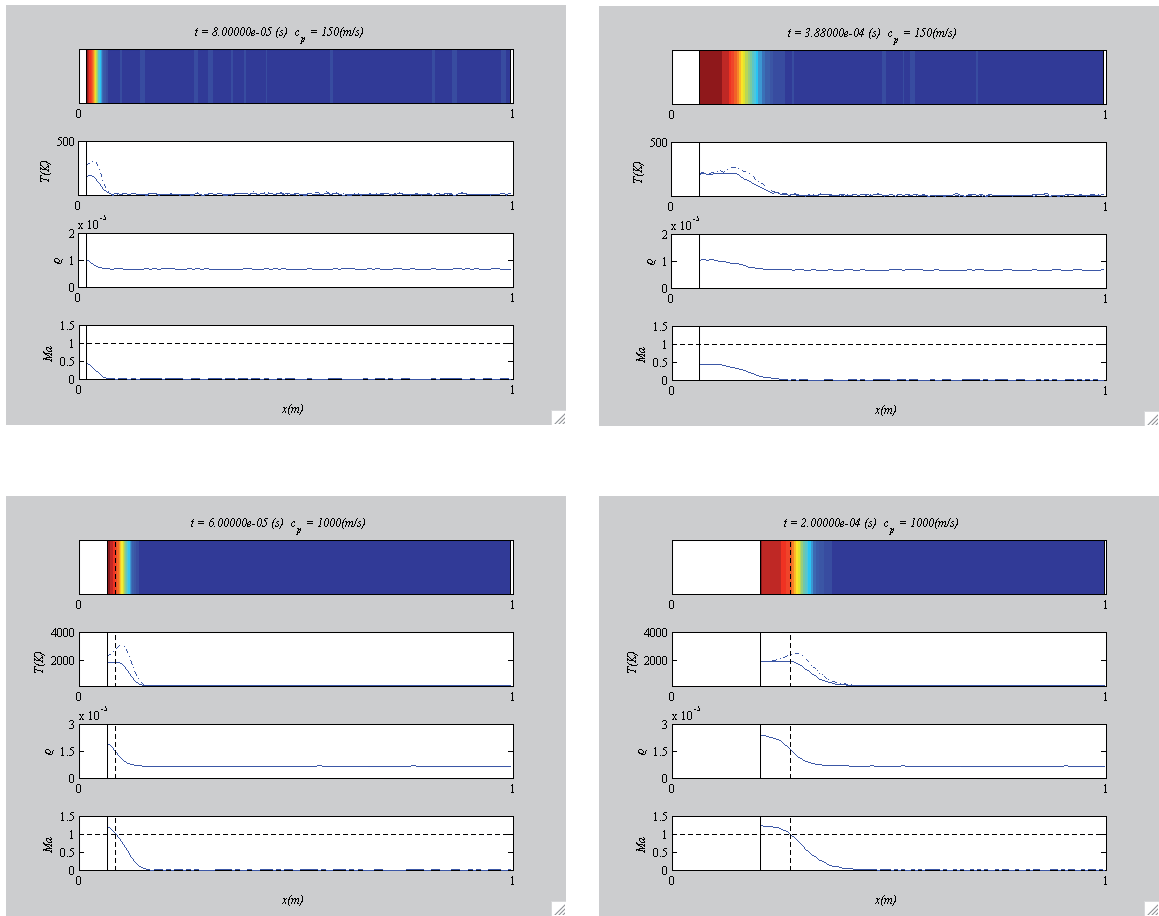


Figure 3: Velocity contours, temperature, density and Mach number along the pipe at $M_p = 0.5$ (upper figures) and $M_p = 3.3$ (lower figures) at two different times

indicated by the dashed line. However the disturbance region still increases with time at a speed that is predicted by normal shock relations.

References

ANDERSSON, J. D. 2003 *Modern Compressible Flow: With Historical Perspective*, 3rd edition. McGraw-Hill Higher Education.

RELAXATION IN A GAS WITH VIBRATIONAL EXCITATION

MARGARITA SASS-TISOVSKAYA margst@nada.kth.se

QIANG LI qiang@mech.kth.se

5C5105, part III: Gas Kinetic Theory

Advisor: Anders Dahlkild and Lars Söderholm

1 Introduction

As we know that a diatomic molecule has several modes of energy: translational energy, rotational energy, vibrational energy and electronic energy. In this project, we are looking at the energy associated with vibrational mode. For a diatomic molecule, vibration is modelled by a spring connecting the two atoms, as illustrated in Figure 1.

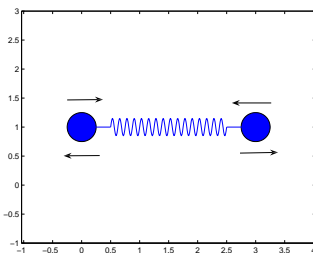


Figure 1: The spring model of the vibrational energy mode.

In this project we examined the relaxation in a gas with vibrational excitation through numerical simulation. Vibrational energy relaxation, or vibrational population relaxation, is a process in which the population distribution of molecules in vibrationally quantum states of high energy level returns to the Boltzmann distribution due to collisions.

The Larsen-Borgnakk model, see Bird (1994) for more detail, is adopted to the vibrational modes through either a classical procedure that assigns a continuously distributed vibrational energy to each molecule, or through a quantum approach that assigns a discrete vibrational level to each molecule.

2 DSMC

The simulation code we choose is DSMC0V.FOR which is concerned with the modelling of vibrational excitation. Some parameters are summarised in Table 1.

| | |
|--|--------|
| number of cell and sub-cells per cell | 1 |
| number of "particles" | 1.E5 |
| number density | 1.E20 |
| simulated region | 0-1 m |
| translational temperature | 5000 K |
| characteristic vibrational temperature | 2000 K |

Table 1: Parameters for the direct numerical simulation.

3 Results

We first ran cases with the initial rotational and vibrational temperatures being chosen to the same value as the translational temperature. The time-averaged values for the overall, translational, rotational and vibrational temperatures are essentially the same. Also the sampled vibrational distribution function at $T = 5000K$ shown in Figure 2 is in excellent agreement with the Boltzmann distribution.

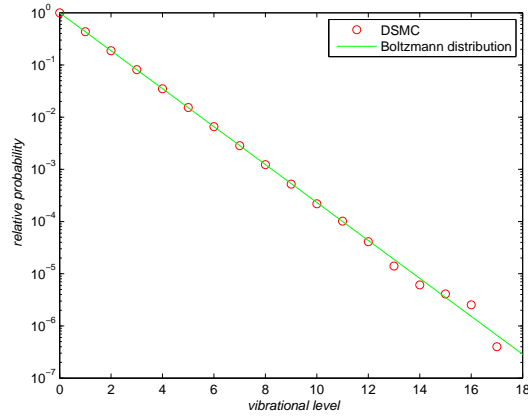


Figure 2: The distribution function of the vibrational states in a gas with $\Theta_v = 2000K$ at a temperature of $5000K$.

The effective number of degrees of freedom of vibration in the test are also shown in Figure 3 compared with the theoretical values. The agreement is in expected statistical scatter.

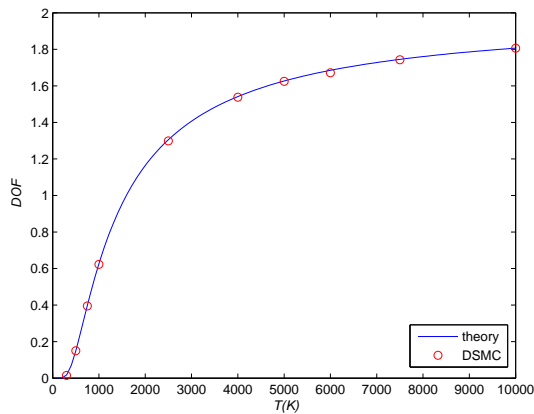


Figure 3: The distribution of the effective number of degrees of freedom of vibration in a gas with $\Theta_v = 2000K$.

Another two cases with the initial rotational and vibrational tempera-

tures set to zero while the translational temperature is $5000K$ were run to examine the effect of the vibrational relaxation collision numbers.

From the results, we found that both the average temperatures of the separate modes and the vibrational distribution function were indistinguishable from those for corresponding case with a constant vibrational relaxation collision number.

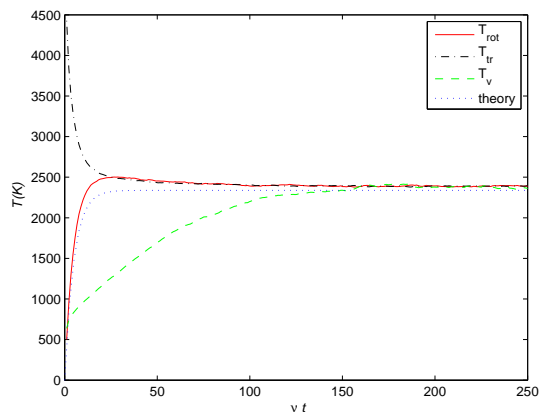


Figure 4: Vibrational relaxation with temperature dependent rate.

The result from the temperature dependent collision number test case is shown in Figure 4. As seen from the plot, the rotational mode quickly comes to equilibrium as well as the translational mode, while the vibrational relaxation grows slowly. The time-averaged T_{all} is $2392K$, while T_{tr} , T_{rot} and T_{vib} are $2389K$, $2390K$, and $2401K$, respectively. More importantly, the distribution function for the vibrational energy is again in excellent agreement with the Boltzmann distribution.

References

- J. D. Anderson. *Modern Compressible Flow : With Historical Perspective*. McGraw-Hill, New York, U.S.A., 2nd edition, 1990.
- G. A. Bird. *Molecular Gas Dynamics and the Direct Simulation of Gas Flows*. Clarendon Press, Oxford, U.K., 1994.

Bulk viscosity in normal shock waves

Linus Marstorp
Outi Tammissola

May 30, 2007

1 Introduction

Bulk viscosity is usually neglected in the continuum derivation of the Navier Stokes equation. In fact, it is zero in a monoatomic gas since bulk viscosity requires at least two degrees of rotational freedom. In the continuum limit the bulk viscosity appears as an isotropic contribution to the viscous stress

$$\sigma_{ij} = 2\mu S_{ij}^{dev} + \frac{\partial u_k}{\partial x_k} \kappa \delta_{ij} \quad (1)$$

where S_{ij}^{dev} is the traceless part of the strain rate tensor, and κ is the bulk viscosity coefficient. From eq (1) we see that bulk viscosity can only appear in compressible ($\nabla \cdot u \neq 0$) flows. Significant bulk viscosity requires a highly compressible flow, such as a shock wave of a diatomic gas.

It is the non-equilibrium of the rotational temperature that gives rise to bulk viscosity. A large time scale of the rotational temperature will increase κ . Vincenti and Kruger (1965) claims that κ is proportional to the rotational thermal energy per unit volume, $\rho e c_{v_{rot}}/c_v$, and the mean relaxation time, τ_r , for the rotational energy.

$$\kappa \sim \left(\rho e \frac{c_{v_{rot}}}{c_v} \right) \tau_r$$

2 Results

The effect of rotational relaxation on shock wave structure was investigated by simulations with the Direct Simulation Monte Carlo-method using the code of Bird (1994). The rotational relaxation time τ_r was varied by changing the *rotational collision number* Z_r , *i.e.* the average number of collisions needed for a certain molecule to “reach equilibrium”¹. The connection between τ and Z_r can thus be written simply as:

$$\tau_r = \tau Z_r \quad (2)$$

¹In fact, Z_r is the number of collisions needed for the rotational velocities to advance towards their equilibrium distribution by $1/e$, and τ_r is the corresponding time.

where τ is the mean time between collisions.

Simulations were performed with the parameter values of nitrogen² (N_2) in room temperature (Bird, 1994). Nitrogen is a diatomic molecule with a collision number of 5.5 in room temperature. In the present study, however, the collision number Z_r was artificially varied between 0 and 10.

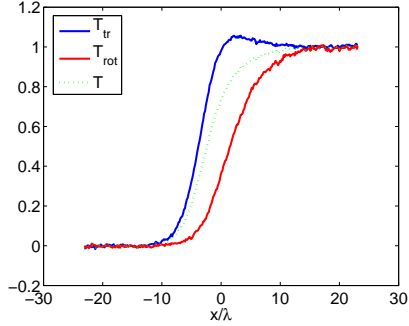


Figure 1: Translational (T_{tr} , blue) and rotational (T_{rot} , red) temperatures as functions of the streamwise coordinate x for rotational collision number $Z_r = 10$.

If Z_r is larger than the number of collisions required to reach the translational equilibrium, Z_{tr} , there is initially too much energy in the translational mode. In fig. 1 it can be seen that after the arrival of the shock the translational temperature rises quicker than the rotational, and overshoots its equilibrium value, whereafter the extra energy is released to the rotational modes by collisions.

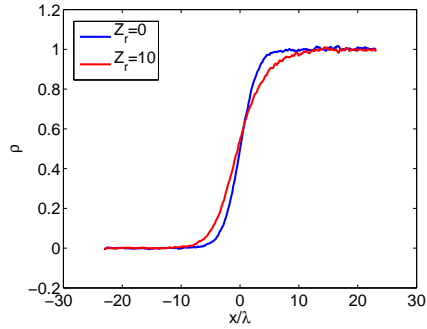


Figure 2: Normalised density distribution as a function the streamwise coordinate x two different rotational collision numbers: $Z_r = 0$ (blue) and $Z_r = 10$ (red).

This dilatational effect can even be seen the structure of shock velocity and

²This means molecular parameters such as molecular diameter and variable soft sphere scattering parameter

density profiles. The effect is similar to that of an increased viscosity - the profiles become smoother and more “smeared out” due to rotational effects. For the same velocity jump, shock thickness based on velocity is inversely proportional to viscosity (Kundu and Cohen, 2004).

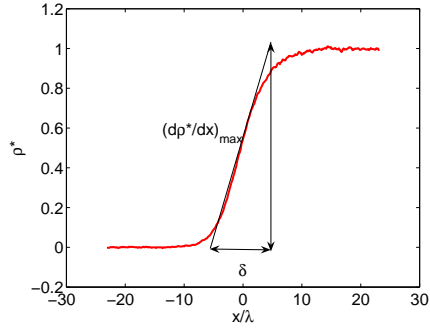


Figure 3: Definition of the normalised shock thickness $\delta = \frac{1}{(\frac{\partial p}{\partial x})_{max}}$.

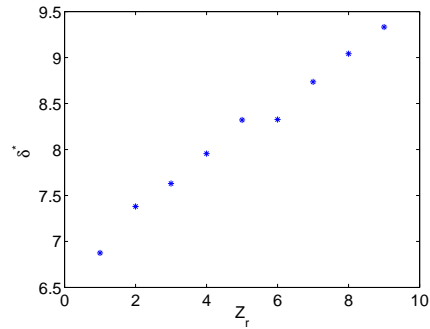


Figure 4: Shock thickness δ (for definition see fig. 3) as a function of rotational collision number Z_r .

Here shock thickness based on the maximum slope of the density profile is studied (for illustration see fig. 3) and shock thickness is found to increase almost linearly with the collision number (fig. 4). This is logical, since bulk viscosity is linearly proportional to the relaxation time.

References

G.A. Bird. *Molecular Gas Dynamics and the Direct Simulation of Gas Flows*, chapter Appendix A. Oxford university press, 1994.

P. Kundu and I.M. Cohen. *Fluid Mechanics*, chapter 16,6, pages 709–710. Elsevier Academic Press, third edition, 2004.

W.G. Vicenti and C.H. Kruger. *Introduction to Physical Gas Dynamics*, chapter X, pages 35–56. John Wiley & Sons, Inc., reprint 1986 edition, 1965.

Direct Simulation Monte Carlo Method of a rarified gas in a pipe with ditches 5C5105, part III, 2007

Gabrielle Bellani and Ramis Örlü
e-mail: bellani@mech.kth.se and ramis@mech.kth.se

May 25, 2007

1 Introduction

The thermal creep flow and the related one-way flow in a pipe with ditches for Knudsen numbers around unity were computed by means of the Direct Simulation Monte Carlo Method. The effect of the geometry of the ditches and the Knudsen number were investigated in order to optimise the pumping ability of the system.

2 Theory

In the continuum approach, where the Navier-Stokes equations are applicable, the no-slip boundary condition is generally applied to a solid surface. Such a condition does not allow the establishment of any non-zero stationary velocity, in the absence of external forces or a pressure gradient. In the case of a rarified gas, however, there can be an appreciable slip velocity at the wall, so that the boundary condition becomes

$$u|_{wall} = u_{wall} + u_{slip}. \quad (1)$$

When a temperature gradient in the tangential direction (t) is present in the gas the slip velocity is given by

$$u_{slip} = \mu_T (\nabla T)_t, \quad (2)$$

where $\mu_T \sim c_s \frac{\lambda}{T}$ denotes the thermal creep velocity coefficient. Hereby λ , c_s and T are the mean free path, the speed of sound and the temperature, respectively. Hence, a flow in the direction of the temperature gradient, in a region of order λ near the boundary, is established. When the mean free path is comparable with the dimensions of the characteristic length scale, (i. e. $Kn = \mathcal{O}(1)$) the slip velocity can be large and exploited for practical applications. The interested reader can find a more detailed explanation of this phenomena in [1,2] and in the lecture notes.

3 Geometry and Numerical parameters

The aim of the present project was to investigate the flow induced by thermal creep in a pipe with ditches with periodically applied temperature gradients at the walls, as depicted in figure 1. The pipe length was $L = 2m$ and the diameter was set to $D = 1m$, whereas the ditch depth, d , and width, b , where the variables to be optimised. The effect of the temperature ratio and the Knudsen number were also investigated.

For the DSMC simulation a PC program (DS2G) was used instead of the Fortran code, because the temperature gradient at the wall could not be easily implemented.

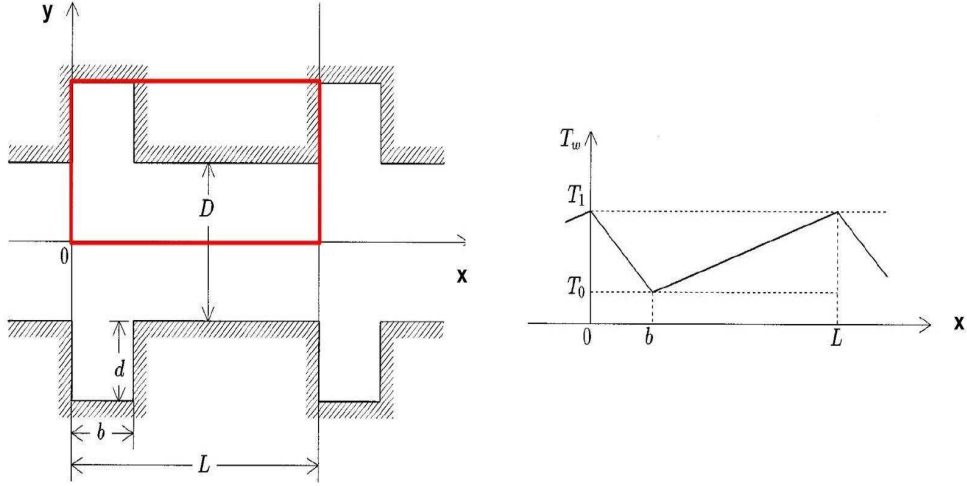


Figure 1: Pipe configuration and temperature distribution at the pipe wall. The red block shows the computational domain.

The DSMC simulation was carried out with the following parameters:

- Gas: Argon
- Timestep: $0.02ms$
- # simulated molecules: 120000
- diffuse reflection
- $T_0 = 300K$
- # sub-cells per region: 20×15

4 Results

The temperature and velocity field for $d/D = b/L = 0.5$, $T_1/T_0 = 3$ and $Kn = 0.1$ is shown in figure 2. A flow in the direction of the temperature gradient is induced in the ditches, but it is blocked by the side walls. Consequently a net flow establishes in the pipe. The computed mass flow rate at this condition was around $0.4g/s$.

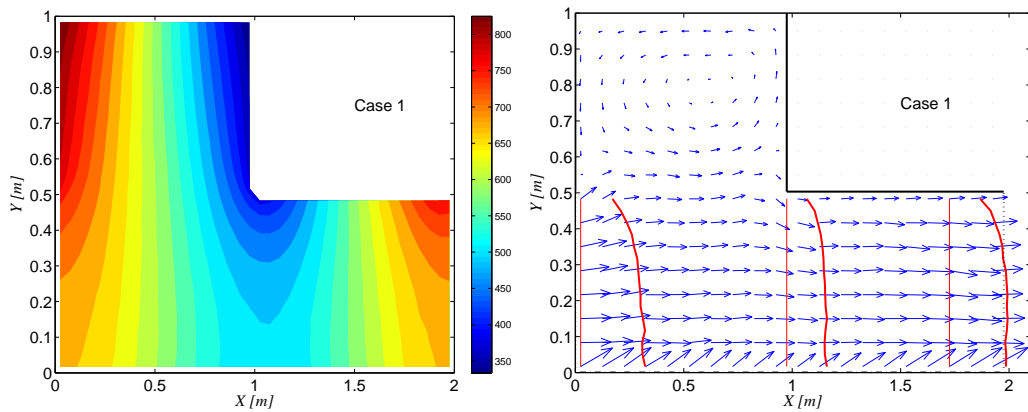


Figure 2: Temperature distribution and velocity vectors after a steady state condition has been reached. Red curves visualise the streamwise velocity profile.

Different configurations in terms of geometry, temperature ratios and Knudsen numbers were tested, and the results are shown in figure 3.

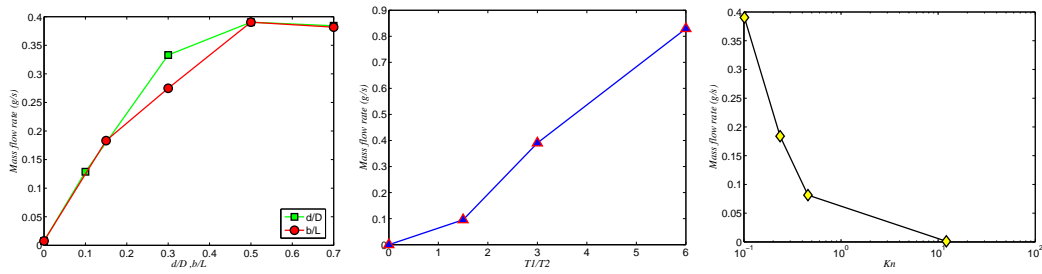


Figure 3: The mass flow rate is plotted as a function of the ditch depth and width ratio, the temperature ratio and the Knudsen number in the leftmost, centred and rightmost figures, respectively. The maximum mass flow rate was found to be at $d/D = b/L = 0.5$ and $Kn = 0.1$, and it increased with increasing temperature ratio.

References

- [1] Sone et al., Phys. Fluids, **8**, pp. 2227-2235 (1996)
- [2] Aoki et al., Rarefied Gas Dynamics: 22nd Int. Symp., pp. 940-947 (2001)